pounds, edited by M. Aven and J. S. Prener (Wiley, New York, 1967), p. 119.
[11]M. Aven and J. A. Parodi, J. Phys. Chem. Solids 13, 56 (1960).
[12]W. Low and M. Weger, Phys. Rev. 118, 1119 (1960); 118, 1330 (1960).
[13]Recent work by J. Vallin and G. A. Slack indicates that two lines close to 10 and 11 originate from cubic sites (unpublished).
[14]W. G. Spitzer, in *Semiconductors and Semimetals*, edited by R. K. Willardson and A. C. Beer (Academic, New York, 1967), Vol. 3, p. 17.
[15]H. D. Fair, Jr., R. D. Ewing, and F. E. Williams, Phys. Rev. 144, 298 (1966).
[16]F. E. Williams, in *International Symposium on Luminescence*, edited by N. Riehl and H. Kallmann (Thiemig, Munich, 1965), p. 332.

PHYSICAL REVIEW B VOLUME 2, NUMBER 1 1 JULY 1970

Theoretical Study of the Raman Relaxation of Ni^{2+} and Cr^{3+} Ions in MgO Crystals

D. K. Ray and T. Ray
Faculté des Sciences, Laboratoire de Spectromètrie Physique, Cedex 53, 38-*Grenoble, France*
and
M. J. L. Sangster
J. J. Thomson Physical Laboratory, Reading, United Kingdom
and
S. K. Gupta
Saha Institute of Nuclear Physics, Calcutta-9, *India*
(Received 11 November 1969)

The Raman relaxation rates for Ni^{2+} and Cr^{3+} ions in MgO crystals have been calculated using a shell model of phonons which is in good agreement with the results of neutron scattering experiments. These shell-model results are compared with those obtained with the Debye model for the phonons and, also, with the available experimental results for Ni^{2+} and Cr^{3+} in MgO. In the case Ni^{2+}, 50 °K is the highest temperature for which the relaxation time is sufficiently long to be directly measureable. As might be expected, in this low-temperature region the results based on the shell model and the Debye model of phonons are not significantly different. However, the values of relaxation rates at 123 and 136 °K obtainable from the recent line-shape measurements for Ni^{2+} in MgO are in good agreement with those calculated on the basis of the shell model of phonons. In the case of Cr^{3+} ions, the relaxation time can be measured directly up to temperatures as high as 200 °K, and in this range of temperature the two sets of results differ considerably. With the shell model, we obtain good agreement with the experimental results on the functional dependence of the relaxation rate $1/T_1$ on temperature. However, the absolute values of $1/T_1$ for Cr^{3+} obtained with this phonon model are on the average less than the experimental measurements by a factor of 5. The possible sources which might be important in bridging the gap between the theoretical and experimental results are discussed.

I. INTRODUCTION

It is well known that when spin-resonance transitions are induced in a paramagnetic crystal by applying external microwave power, the spin system then relaxes through the dissipation of energy to the lattice. In the single-phonon process, the spin-lattice relaxation amounts to the creation of phonons of energy equal to the energy of the spin transitions, whereas, in the only important two-phonon process, two phonons simultaneously take part – one being annihilated and another being creating, conserving the net energy. Obviously, in the two-phonon process, the entire phonon spectrum will be involved and consequently, at higher temperatures, two-phonon processes are expected to be important in the relaxation mechanisms. The relative importance of the high-frequency phonons will depend on the temperature at which the relaxation is measured. Most paramagnetic ions have relaxation times too short to be measured directly above the liquid-nitrogen temperature, so that only the effects of phonons of relatively small frequencies (<100 cm^{-1}) can be studied by means of resonance techniques. In explaining the data from the specific heat experiments, the Debye model is found to give a fairly good description of the low-frequency phonons.[1] Hence,

in the measurements of the relaxation times for most paramagnetic ions, the results are expected to agree well with the long-wavelength approximation,[2] and Debye T^9 and T^7 laws are found to be well satisfied for Kramers and non-Kramers ions, respectively. For example, the measurements done by Williams[3] on Co^{2+} in MgO shows that $1/T_1$ varies as $T^{8.5}$ in the temperature range 12 to 20 °K. Recent experiments on some rare-earth ions by Huang[4] and Larsen and Jeffries[5] show that the Raman relaxation varies with temperature as T^9 for Kramers ions, and for non-Kramers ions such as Tb^{3+} in yttrium-ethyl sulfate, the T^7 law is well satisfied. Considering the absolute magnitude, there is, in general, a difference of one to two orders of magnitude between the experimental values and those calculated theoretically assuming an effective point-charge model of the ligand charge distributions. The difference is usually attributed[6] to the approximations involved in the effective point charge model.

Fortunately, there are a few paramagnetic ions which have the first excited levels well above an orbitally nondegenerate ground level so that the resulting spin-orbit and, hence, the spin-phonon coupling are sufficiently weak in these cases. For these ions it is possible to measure the relaxation time up to temperatures high enough for the high-frequency phonons to be more appreciably involved. For such cases, deviations from the T^7 law are expected to be significant. Recent experiments on Cr^{3+} and Fe^{3+} in MgO crystals[7,8] confirm this behavior. Also, neutron scattering experiments on MgO crystals[9] indicate marked differences in the phonon distribution from that expected from the Debye model, particularly, for the high-frequency phonons. For Ni^{2+} in MgO, information about the relaxation rates at high temperatures from line-shape measurements is now available.[10] In this paper, we have analyzed the importance of the model used for the phonon characteristics on the Raman relaxation rates in Ni^{2+} and Cr^{3+} ions in MgO crystal. We have done this by calculating the magnitude and the dependence on temperature of the relaxation time assuming the real phonon model – by which term we mean a shell model which has been found to give good agreement with the results of neutron scattering experiments – and comparing them with the experimental results, where available, and with the theoretical results obtained for the Debye model of phonons. In the case of Ni^{2+}, the spin-phonon coupling is strong, and consequently, direct measurements of spin-lattice relaxation rates are possible only up to about 50 °K. As the effect of the high-frequency phonons is not expected to be important in this temperature region, the theoretical results calculated with the real phonon model should not differ significantly from those calculated with the Debye model. But the spin-lattice relaxation rates which have been calculated at 123 and 136 °K from the line-shape measurements[10] should involve high-frequency phonons and consequently it will be interesting to compare these results with those given by the real phonon model and the Debye model.

The possibility of making direct measurements of the relaxation times at sufficiently high temperatures makes the case of Cr^{3+} an interesting one to study from the point of view of assessing the effect of a more realistic description of the phonons than is given by the Debye model, on both the magnitude and temperature dependence of the relaxation time. In Sec. II, we shall discuss the general method of calculating the transition probability that we have followed, and in the course of formulating the general method, a very simple and useful way of evaluating the orbit-lattice interaction parameters in any complex, using an effective point-charge model for the ligand ions, is discussed. The application of the general method to the cases of Ni^{2+} and Cr^{3+} in an XY_6 complex is given in Sec. III. It should be noted that we have considered all possible symmetrized displacements of the ligands in the XY_6 complex, of both odd and even parity, and it is interesting that in the two-phonon relaxation mechanisms, the rotation-type symmetrized displacements and those belonging to odd parity are as important as the Γ_{3g} and Γ_{5g} modes considered in an earlier work.[11] In this section, we shall also discuss the procedure for calculating the phonon integrals that are needed in the evaluation of the transition probability. In the same section, we discuss the results which we obtained with the real phonon model and compare them with the corresponding values calculated with the Debye model. It is noteworthy that (i) for the case of Ni^{2+}, as is anticipated, the results with the real phonon model do not differ significantly from the values with the Debye model of phonons up to about 100 °K. The available experimental results at 123 and 136 °K are in good accord with the real phonon results; (ii) for the case of Cr^{3+}, the experimental results on the variation of T_1 with temperature which deviate widely from the theoretical T^7 law, as predicted by the Debye model, are well explained by the real phonon model.

The calculations presented in this paper are done under the assumption of the perfect MgO lattice, i.e., no account is taken of the mass difference of the impurity ion or of the distortions and force-constant changes which it introduces on the lattice. It would be interesting to see how much the results

are affected in the phonon model were to include the changes in the lattice introduced by the substitution of the paramagnetic ion in the crystal.

II. GENERAL METHOD OF CALCULATING TRANSITION PROBABILITY USING DYNAMICAL HAMILTONIAN FORMALISM

For paramagnetic systems with spin $1 \leq S < 2$, and considering only the two phonon processes, we can write the dynamical Hamiltonian[11] as follows:

$$\mathcal{H}_{\rm dyn} = \sum_{\alpha,\beta,\gamma,i,j,l} C(\alpha:\beta,\gamma)\langle \Gamma^i_{\alpha g} \mid \Gamma^j_\beta, \Gamma^l_\gamma\rangle \times S_2(\Gamma^i_{\alpha g}) Q(\Gamma^j_\beta)\, Q(\Gamma^l_\gamma), \quad (1)$$

where $C(\alpha:\beta,\gamma)$ are the spin-phonon coupling parameters, $S_2(\Gamma^i_{\alpha g})$ are symmetrized spin operators, and the phonon operators Q are the symmetry-adapted displacements of the particular complex formed by the ligand charge distributions around the paramagnetic ion site. Next we transform the symmetry modes to the lattice modes of the crystal by using the following relation:

$$Q(\Gamma^j_\beta) = \textstyle\sum_s A(\Gamma^j_\beta : s)\, q(s) \ , \quad (2)$$

where s is the index for the generalized mode of the phonons; $q(s)$ are the phonon operators defined in Eqs. (A4) and (A5) of the Appendix. The coefficients $A(\Gamma^j_\beta : s)$ correlate a particular symmetry coordinate $Q(\Gamma^j_\beta)$ to the phonon of generalized mode s. Also, we use the following substitution for the spin operators $S_2(\Gamma^i_{\alpha g})$:

$$S_2(\Gamma^i_\alpha) = \textstyle\sum_\mu D_2^{\Gamma^i_\alpha,\mu}(S)^\mu_2 \ , \quad (3)$$

where D_2 are the rotation group matrices of rank 2, and $(s)^\mu_2$ is μth component of the spin tensor of rank 2. For Raman processes, the Hamiltonian in Eq. (1), therefore, reduces to

$$\mathcal{H}_{\rm dyn} = \sum_{s,s',\mu} B^\mu_{s,s'} (S)^\mu_2 \times (b_s b^\dagger_{s'} + b^\dagger_s b_{s'} + b_{-s} b^\dagger_{-s'} + b^\dagger_{-s} b_{-s'}) \ , \quad (4)$$

where

$$B^\mu_{s,s'} = \frac{\hbar}{4}\left(\frac{1}{\omega_s \omega_{s'}}\right)^{1/2} \sum_{\alpha,\beta,\gamma,i,j,l} C(\alpha:\beta,\gamma)\langle \Gamma^i_\alpha \mid \Gamma^j_\alpha, \Gamma^l_\gamma\rangle \times D_2^{\Gamma^i_\alpha,\mu} A(\Gamma^j_\beta : s) A(\Gamma^l_\gamma : s') \ . \quad (5)$$

Remembering that the representation Γ_α and Γ_β can possibly occur more than once in the symmetry under consideration, Eq. (5) should be written in the more general form

$$B^\mu_{s,s'} = \frac{\hbar}{4}\left(\frac{1}{\omega_s \omega_{s'}}\right)^{1/2} \sum_{\alpha,\beta,\gamma,i,j,l,n,n'} C(\alpha : n\beta, n'\gamma) \times \langle \Gamma^i_\alpha \mid \Gamma^j_\beta, \Gamma^l_\gamma\rangle D_2^{\Gamma^i_\alpha,\mu} A({}^n\Gamma^j_\beta : s) A({}^{n'}\Gamma^l_\gamma : s'), \quad (6)$$

where the indices n, n' differentiate between the occurrences of the same representation. For the transition probability due to the Raman process, we then have

$$W_{M_s+\mu \to M_s} = \frac{8\pi}{\hbar} \mid \langle M_s + \mu \mid (S)^\mu_2 \mid M_s\rangle \mid^2 \sum_{s,s'} \bar{n}_s(\bar{n}_{s'}+1) \times \mid B^\mu_{s,s'} \mid^2 \delta(\hbar\omega_s - \hbar\omega_{s'}) \ , \quad (7)$$

where we assume $g\beta H \ll \hbar\omega_s$ and where n_s is the number of phonons of the generalized s mode at thermal equilibrium. A simplification of Eq. (7) may be made from the following symmetry considerations. The frequency ω_s corresponding to the sth normal mode of the crystal (including the impurity) is not in general unique, since a set of normal modes may be generated from the sth mode by the symmetry operations for the (imperfect) crystal. We may, therefore, divide the summation over s (and s') into two parts, namely, (i) a summation over all nonequivalent modes, and (ii) a summation over all symmetry operations for the crystal, which must take due account of the fact that the number of distinct normal modes generated may be less than the number of symmetry operations. Equation (7) may, therefore, be rewritten as follows:

$$W_{M_s+\mu \to M_s} = (8\pi/\hbar) \mid \langle M_s + \mu \mid (S)^\mu_2 \mid M_s\rangle \mid^2 \times \sum_{s_1, s_1'} \bar{n}_{s_1}(\bar{n}_{s_1'}+1)\, \delta(\hbar\omega_{s_1} - \hbar\omega_{s_1'}) \times \sum_{\text{symm. opr.}} \mid B^\mu_{s_1,s_1'} \mid^2 \ . \quad (8)$$

The summation variables s_1 and s_1' are now over nonequivalent normal modes, and we have used the fact that the factor $\bar{n}_s(\bar{n}_{s'}+1)$ is constant for all terms generated in the summation over the symmetry operations. It should perhaps be stressed at this point that, despite the δ function in Eq. (7), a normal mode s' cannot be generated from a normal mode s by a symmetry operation since their frequencies differ by the energy $g\beta H$. From Eq. (6), we have

$$\sum_{\text{symm.opr.}} \mid B^\mu_{s_1,s_1'} \mid^2 = \frac{\hbar^2}{8}\frac{1}{\omega_{s_1}\omega_{s_1'}} \sum \langle \Gamma^i_\alpha \mid \Gamma^j_\beta, \Gamma^l_\gamma\rangle \times \langle \Gamma^{i'}_{\alpha'} \mid \Gamma^{j'}_{\beta'}, \Gamma^{l'}_{\gamma'}\rangle C(\alpha : n\beta, n'\gamma)\, C(\alpha' : n''\beta', n'''\gamma) \times D_2^{\Gamma^i_\alpha,\mu} D_2^{\Gamma^{i'}_{\alpha'},\mu} \sum_{\text{symm. opr.}} A({}^n\Gamma^j_\beta : s_1) A({}^{n''}\Gamma^{j'}_{\beta'} : s_1) \times A({}^{n'}\Gamma^l_\gamma : s_1') A({}^{n'''}\Gamma^{l'}_{\gamma'} : s_1') \ . \quad (9)$$

By using the orthogonality condition of the sym-

metry modes Q, one can show that

$$\sum_{\text{symm. opr.}} A({}^{n}\Gamma_{\beta}^{j} : s_1)\, A({}^{n''}\Gamma_{\beta'}^{j'} : s_1) = 0$$

$$\text{for } \beta \neq \beta', \qquad j \neq j' \tag{10}$$

and that it is independent of the component j. We can then make use of the orthogonality relation between the Clebsch-Gordan (CG) coeffieients, namely,

$$\sum_{j,l} \langle \Gamma_{\alpha'}^{i'} \mid \Gamma_{\beta}^{j}, \Gamma_{\gamma}^{l} \rangle \langle \Gamma_{\alpha}^{i} \mid \Gamma_{\beta}^{j}, \Gamma_{\gamma}^{l} \rangle = 0$$

$$\text{if } \alpha \neq \alpha', \qquad i \neq i' \quad . \tag{11}$$

These two conditions reduce Eq. (9) to the following:

$$\sum_{\text{symm.opr.}} \left| B_{s_1, s_1'}^{\mu} \right|^2 = \frac{\hbar^2}{8} \frac{1}{\omega_{s_1}\omega_{s_1'}}$$

$$\times \sum_{\alpha,\beta,\gamma,i,j,l} \left| \langle \Gamma_{\alpha}^{i} \mid \Gamma_{\beta}^{j}, \Gamma_{\gamma}^{l} \rangle \right|^2$$

$$\times \left| D_2^{\Gamma_{\alpha}^{i},\mu} \right|^2 C(\alpha : n\beta, n'\gamma)\, C(\alpha : n''\beta, n'''\gamma)$$

$$\times R_{\Gamma_{\beta}}^{nn''}(s_1)\, R_{\Gamma_{\gamma}}^{n'n'''}(s_1') \quad , \tag{12}$$

where we define the symbol $R_{\Gamma_{\beta}}^{nn'}(s)$ as follows:

$$R_{\Gamma_{\beta}}^{nn'}(s) = \sum_{\text{symm.opr.}} A({}^{n}\Gamma_{\beta} : s)\, A({}^{n'}\Gamma_{\beta} : s) \quad . \tag{13}$$

The transition probability will then be given by

$$W_{M_S+\mu \to M_S} = \pi\hbar \left| \langle M_S + \mu \mid (S)_2^{\mu} \mid M_S \rangle \right|^2$$

$$\times \sum_{\alpha,\beta,\gamma,i,j,l} \left| \langle \Gamma_{\alpha}^{i} \mid \Gamma_{\beta}^{j}, \Gamma_{\gamma}^{l} \rangle \right|^2 \left| D_2^{\Gamma_{\alpha}^{i},\mu} \right|^2 C(\alpha : n\beta, n'\gamma)$$

$$\times C(\alpha : n''\beta, n'''\gamma) \sum_{s_1, s_1'} \frac{1}{\omega_{s_1}\omega_{s_1'}} (\bar{n}_{s_1} + 1)\, \bar{n}_{s_1'}\, R_{\Gamma_{\beta}}^{nn''}(s_1)$$

$$\times R_{\Gamma_{\gamma}}^{n'n'''}(s_1')\, \delta(\hbar\omega_{s_1} - \hbar\omega_{s_1'}) \quad . \tag{14}$$

The R functions are reexpressed in terms of smooth frequency functions given by the relation

$$R_{\Gamma_{\beta}}^{nn'}(\omega_s)\, \Delta\omega = \sum_{\substack{\text{over all } s \text{ such} \\ \text{that } \omega \leq \omega_s \leq \omega + \Delta\omega}} R_{\Gamma_{\beta}}^{nn'}(s) \quad . \tag{15}$$

For the perfect lattice case, these functions can be calculated directly. But, it is convenient to re-express these functions in terms of the classical Green's functions for the lattice. The corresponding calculations for the case of the lattice with modifications of mass and force constants may be performed by introducing the effects of such modifications through the Lifshitz formalism.[12] Defining a Green's function as follows[13]:

$$G_{\Gamma}^{nn'}(\omega) = \lim_{\epsilon \to 0} \int_0^{\infty} \frac{R_{\Gamma}^{nn'}(\omega')}{\omega'^2 - \omega^2 + i\epsilon\omega}\, d\omega' \quad , \tag{16}$$

we get $\quad \text{Im}\, G_{\Gamma}^{nn'}(\omega) = -(\pi/2\omega)\, R_{\Gamma}^{nn'}(\omega) \quad . \tag{17}$

Using Eqs. (15) and (17) in Eq. (14), we get the following expression for the transition probability:

$$W_{M_S+\mu \to M_S} = \frac{4\hbar}{\pi} \left| \langle M_S + \mu \mid S_2^{\mu} \mid M_S \rangle \right|^2$$

$$\times \sum_{\alpha,\beta,\gamma,i,j,l} \left| \langle \Gamma_{\alpha}^{i} \mid \Gamma_{\beta}^{j}, \Gamma_{\gamma}^{l} \rangle \right|^2 \left| D_2(\Gamma_{\alpha}^{i}, \mu) \right|^2$$

$$\times C(\alpha : n\beta, n'\gamma)\, C(\alpha : n''\beta, n'''\gamma) \int (\bar{n}_{s_1} + 1)\, \bar{n}_{s_1'}$$

$$\times \text{Im}\, G_{\Gamma_{\beta}}^{nn''}(\omega_{s_1})\, \text{Im}\, G_{\Gamma_{\gamma}}^{n'n'''}(\omega_{s_1'})\, d\omega_{s_1}\, d\omega_{s_1'}$$

$$\times \delta(\hbar\omega_{s_1} - \hbar\omega_{s_1'}) \quad . \tag{18}$$

Substituting in Eq. (18) the boson distribution function for n_s and defining integrals I as follows:

$$I(\Gamma_{\beta}, nn''; \Gamma_{\gamma}, n'n'''; T) = \int \frac{e^{\hbar\omega/kT}}{[e^{\hbar\omega/kT} - 1]^2}$$

$$\times \text{Im}\, G_{\Gamma_{\beta}}^{nn''}(\omega)\, \text{Im}\, G_{\Gamma_{\gamma}}^{n'n'''}(\omega)\, d\omega, \tag{19}$$

we arrive at the following final expression for the transition probability:

$$W_{M_S+\mu \to M_S} = (4/\pi) \left| \langle M_S + \mu \mid S_2^{\mu} \mid M_S \rangle \right|^2$$

$$\times \sum_{\alpha,\beta,\gamma,i,j,l} \left| \langle \Gamma_{\alpha}^{i} \mid \Gamma_{\beta}^{j}, \Gamma_{\gamma}^{l} \rangle \right|^2 \left| D_2^{\Gamma_{\alpha}^{i},\mu} \right|^2$$

$$\times C(\alpha : n\beta, n'\gamma)\, C(\alpha : n''\beta, n'''\gamma)$$

$$\times I(\Gamma_{\beta}, nn''; \Gamma_{\gamma}, n'n'''; T) \quad . \tag{20}$$

Up to this point no use has been made of the translational symmetry of the perfect lattice, so that the results apply whether or not we ignore the modifications introduced by the impurity ion. In the present work, however, we are interested in the case when such modifications are ignored. The method of evaluating the $\text{Im}G_{\Gamma_{\beta}}$ functions appearing in the I integrals for the case of the perfect lattice is discussed in the Appendix. We next use Eq. (20) to calculate the transition probabilities for Ni^{2+} and Cr^{3+} ions in a perfect MgO crystal. Before considering these specific cases, however, it is necessary to discuss the method of evaluating the spin-phonon coupling constants $C(\alpha : n\beta, n'\gamma)$, which we do in Sec III.

III. METHOD OF EVALUATION OF SPIN-PHONON COUPLING PARAMETERS IN $\mathcal{H}_{\text{dyn}}$

To evaluate the spin-phonon coupling parmeters $C(\alpha : \beta, \gamma)$ in $\mathcal{H}_{\text{dyn}}$, we start from the basic perturbing interactions on the crystal field states, namely,

$$\mathcal{H}^{(1)} = \mathcal{H}_{s\text{-}o} + \mathcal{H}_{o\text{-}l} \quad , \tag{21}$$

where $\quad \mathcal{H}_{s\text{-}o} = \lambda \vec{L} \cdot \vec{S} \tag{22}$

and $$\mathcal{H}_{o\text{-}1}=\sum_{l,\alpha} A_{l,\alpha} r^l \sum_i Y_l^{(e)}(\Gamma_\alpha^i) Q(\Gamma_\alpha^j) + \sum_{l,\alpha,\beta,\gamma} A_{l,\alpha,\beta,\gamma} r^l \sum_{i,j,k} \langle \Gamma_\alpha^i | \Gamma_\beta^j, \Gamma_\gamma^k \rangle \times Y_l^{(e)}(\Gamma_\alpha^i) Q(\Gamma_\beta^j) Q(\Gamma_\gamma^k) \quad (23)$$

neglecting terms of higher order than quadratic in the phonon operators in the orbit-lattice interaction. $Y_l^{(e)}(\Gamma_\alpha^i)$ is the spherical harmonic of rank l which transforms as the ith component of the Γ_αth irreducible representation. The index e signifies the electron on the paramagnetic ion. We can also write

$$\mathcal{H}_{o\text{-}1}=\sum_i \frac{\partial V}{\partial Q_i}\bigg|_{eq} Q_i + \tfrac{1}{2}\sum_{i,j} \frac{\partial^2 V}{\partial Q_i \partial Q_j}\bigg|_{eq} Q_i Q_j \ , \quad (24)$$

where V is the dynamical crystal potential at any instant. Assuming an effective point charge $+Ze$ at the ligand ions, we can write

$$V=-\sum_l \frac{4\pi}{2l+1}\frac{r^l}{R^{l+1}} Ze^2 \sum_{n,\alpha,i} Y_l^{(n)}(\Gamma_\alpha^i) Y_l^{(e)}(\Gamma_\alpha^i) \ . \quad (25)$$

The index n signifies the ligand. R is the instantaneous radius vector of the ligand, and r is the radius vector of the electron from the center of the paramagnetic ion. Thus, the orbit-lattice interaction parameters can be conveniently derived from the following expressions[14] which are obtained from Eqs. (23)–(25):

$$A_{l,\alpha}=-\frac{4\pi}{2l+1} Ze^2 \bigg| \sum_n \frac{\partial}{\partial Q(\Gamma_\alpha^i)} \frac{Y_l^{(n)}(\Gamma_\alpha^i)}{R^{l+1}} \bigg|_{eq} \quad (26)$$

and

$$A_{l,\alpha,\beta,\lambda}=-\frac{2\pi}{2l+1} Ze^2 (\langle \Gamma_\alpha^i | \Gamma_\beta^j, \Gamma_\gamma^k \rangle)^{-1} \times \bigg| \sum_n \frac{\partial^2}{\partial Q(\Gamma_\beta^j)\partial Q(\Gamma_\gamma^l)} \frac{Y_l^{(n)}(\Gamma_\alpha^i)}{R^{l+1}} \bigg|_{eq} \ . \quad (27)$$

With the perturbing Hamiltonians $\mathcal{H}_{s\text{-}o}$ and $\mathcal{H}_{o\text{-}1}$, we evaluate the changes in the ground-state energy and compare this with the expression of $\mathcal{H}_{dyn}$ given in Eq. (1) to derive the relevant constants $C(\alpha:\beta,\gamma)$. It is obvious that to evaluate the constants C which are associated with the quadratic powers in Q, we have to calculate (i) the third-order change in the ground-state energy, considering the second-order effect of $\mathcal{H}_{s\text{-}o}$ and the first-order effect of the term quadratic in Q in $\mathcal{H}_{o\text{-}1}$, namely,

$$(\Delta E)^{(3)}=\sum_p{}' \bigg(-\frac{1}{(E_0-E_p)^2} (\langle 0|\mathcal{H}_{o\text{-}1}|0\rangle |\langle p|\mathcal{H}_{s\text{-}o}|0\rangle|^2 + 2\langle 0|\mathcal{H}_{s\text{-}o}|0\rangle\langle 0|\mathcal{H}_{o\text{-}1}|p\rangle\langle p|\mathcal{H}_{s\text{-}o}|0\rangle) + \sum_q{}' \frac{1}{(E_0-E_p)(E_0-E_q)} (\langle 0|\mathcal{H}_{o\text{-}1}|q\rangle\langle q|\mathcal{H}_{s\text{-}o}|p\rangle \times \langle p|\mathcal{H}_{s\text{-}o}|0\rangle + \langle 0|\mathcal{H}_{s\text{-}o}|q\rangle\langle q|\mathcal{H}_{s\text{-}o}|p\rangle\langle p|\mathcal{H}_{o\text{-}1}|0\rangle + \langle 0|\mathcal{H}_{s\text{-}o}|q\rangle\langle q|\mathcal{H}_{o\text{-}1}|p\rangle\langle p|\mathcal{H}_{s\text{-}o}|0\rangle) \bigg), \quad (28)$$

and (ii) the fourth-order change in the ground-state energy, considering the second-order effect of $\mathcal{H}_{s\text{-}o}$ and the second-order effect of the term linear in Q in $\mathcal{H}_{o\text{-}1}$. For the sake of simplicity, we give the general expression for $(\Delta E)^{(4)}$, keeping the total perturbing Hamiltonian $\mathcal{H}'$, from which the relevant terms are calculated as in the above expression for the third-order energy,

$$(\Delta E)^{(4)}=\sum_p{}' \bigg(-\sum_q{}' \frac{1}{(E_0-E_p)^2(E_0-E_q)} (\langle 0|\mathcal{H}'|q\rangle \times \langle q|\mathcal{H}'|0\rangle\langle 0|\mathcal{H}'|p\rangle\langle p|\mathcal{H}'|0\rangle + \langle 0|\mathcal{H}'|0\rangle\langle 0|\mathcal{H}'|q\rangle\langle q|\mathcal{H}'|p\rangle\langle p|\mathcal{H}'|0\rangle) + \frac{1}{(E_0-E_p)^3} \langle 0|\mathcal{H}'|0\rangle\langle 0|\mathcal{H}'|0\rangle\langle 0|\mathcal{H}'|p\rangle\langle p|\mathcal{H}'|0\rangle + \sum_q{}' \frac{1}{(E_0-E_p)(E_0-E_q)^2} \langle 0|\mathcal{H}'|0\rangle\langle 0|\mathcal{H}'|q\rangle\langle q|\mathcal{H}'|p\rangle \times \langle p|\mathcal{H}'|p\rangle + \sum_q{}' \frac{1}{(E_0-E_p)(E_0-E_q)(E_0-E_r)} \times \langle 0|\mathcal{H}'|r\rangle\langle r|\mathcal{H}'|q\rangle\langle q|\mathcal{H}'|p\rangle\langle p|\mathcal{H}'|0\rangle \bigg) . \quad (29)$$

The perturbation calculations are much simplified if one expresses the orbital wave functions $|0\rangle$, $|p\rangle$, etc., as exact basis functions of the different irreducible representations of the particular point group under consideration, and makes use of the properties of the Clebsch-Gordan coefficients in this symmetry. Thus, defining the orbital states by $|\psi(\Gamma_\nu^v)\rangle$, we can write the general form of the matrix elements for the orbital part of $\mathcal{H}_{o\text{-}1}$, as

$$\langle \psi(\Gamma_\mu^u)|\, Y_l(\Gamma_\alpha^i)\,|\psi(\Gamma_\nu^v)\rangle = \langle \psi(\Gamma_\mu)|\,|\, Y_l(\Gamma_\alpha)\,|\,|\psi(\Gamma_\nu)\rangle \langle \Gamma_\mu^u | \Gamma_\alpha^i, \Gamma_\nu^v\rangle, \quad (30)$$

where the reduced matrix element $\langle \psi(\Gamma_\mu)|\,|\, Y_l \times (\Gamma_\alpha)|\,|\,\psi(\Gamma_\nu)\rangle$ is independent of the component and is evaluated once for any set Γ_μ, Γ_α, Γ_ν of the irreducible representations. $\langle \Gamma_\mu^u | \Gamma_\alpha^i, \Gamma_\nu^v\rangle$ is the Clebsch-Gordan coefficient in the crystal symmetry. Similarly, for $\mathcal{H}_{s\text{-}o}$, the general matrix element is

$$\lambda\langle \psi(\Gamma_\mu^u)|\sum_{\alpha,i} L_1(\Gamma_\alpha^i) S_1(\Gamma_\alpha^i)|\psi(\Gamma_\nu^v)\rangle = \lambda \sum_\alpha \langle \psi(\Gamma_\mu) \times |\,|L_1(\Gamma_\alpha)|\,|\psi(\Gamma_\nu)\rangle \langle \Gamma_\mu^u | \Gamma_\alpha^i, \Gamma_\nu^v\rangle S_1(\Gamma_\alpha^i) \ . \quad (31)$$

The Clebesch-Gordan coefficients for all point-group symmetries are given by Koster *et al.*[15] Knowing these coefficients and using Eqs. (30) and (31), one essentially reduces the number of matrix elements to be calculated.

IV. RAMAN RELAXATION FOR Ni^{2+} AND Cr^{3+} IONS IN PERFECT MgO CRYSTALS

To evaluate the Raman relaxation times for Ni^{2+} and Cr^{3+} ions in perfect MgO crystals, we have to evaluate the transition probabilities $W_{M_S+\mu\to M_S}$ as given by Eq. (20) for these specific cases. For single-spin transition, we get

$$W_{M_S+1\to M_S}=\pi^{-1}(2M_S+1)^2(S+M_S+1)(S-M_S)$$

$$\times[(s_{1g}+s_{1u})+(l^4+m^4+n^4)$$
$$\times(s_{2g}+s_{2u}-s_{1g}-s_{1u})]\ , \qquad (32)$$

and for the double-spin transitions,

$$W_{M_S+2\to M_S}=(4\pi)^{-1}(S+M_s+2)(S+M_s+1)(S-M_s-1)$$
$$\times(S-M_s)\,[(s_{1g}+s_{1u}+3s_{2g}+3s_{2u})$$
$$+(l^4+m^4+n^4)(s_{1g}+s_{1u}-s_{2g}-s_{2u})]\ , \qquad (33)$$

where s_{1g} and s_{2g} contain the contributions from the phonons of the even-parity modes and s_{1u} and s_{2u} contain that from the odd-parity phonons. These summations are defined below,

$$s_{1g}=C^2(3g:1g,3g)I(1g;3g;T)+C^2(3g:3g,3g)$$
$$\times I(3g;3g;T)+C^2(3g:4g,4g)I(4g;4g;T)$$
$$+C^2(3g:4g,5g)I(4g;5g;T)$$
$$+C^2(3g:5g,5g)I(5g;5g;T)\ , \qquad (34)$$

$$s_{2g}=C^2(5g:1g,5g)I(1g;5g;T)+C^2(5g:3g,4g)$$
$$\times I(3g;4g;T)+C^2(5g:3g,5g)I(3g;5g;T)$$
$$+C^2(5g:4g,4g)I(4g;4g;T)+C^2(5g:4g,5g)$$
$$\times I(4g;5g;T)+C^2(5g:5g,5g)I(5g;5g;T)\ , \qquad (35)$$

$$s_{1u}=C^2(3g:{}^1\!4u,{}^1\!4u)I(4u,11;4u,11;T)$$
$$+C^2(3g:{}^2\!4u,{}^2\!4u)I(4u,22;4u,22;T)$$
$$+2C(3g:{}^1\!4u,{}^1\!4u)C(3g:{}^2\!4u,{}^2\!4u)$$
$$\times I(4u,12;4u;12;T)+2C^2(3g:{}^1\!4u,{}^2\!4u)$$
$$\times[I(4u,11;4u,22;T)+I(4u,12;4u,12;T)]$$
$$+4C(3g:{}^1\!4u,{}^1\!4u)C(3g:{}^1\!4u,{}^2\!4u)I(4u,11;4u,12;T)$$
$$+4C(3g:{}^2\!4u,{}^2\!4u)C(3g:{}^1\!4u,{}^2\!4u)I(4u,22;4u,12;T)$$
$$+2C^2(3g:{}^1\!4u,5u)I(4u,11;5u;T)$$
$$+2C^2(3g:{}^2\!4u,5u)I(4u,22;5u;T)$$
$$+4C(3g:{}^1\!4u,5u)C(3g:{}^2\!4u,5u)I(4u,12;5u;T)$$
$$+C^2(3g:5u,5u)I(5u;5u;T)\ , \qquad (36)$$

and

$$s_{2u}=C^2(5g:{}^1\!4u,{}^1\!4u)I(4u,11;4u,11;T)$$
$$+C^2(5g:{}^2\!4u,{}^2\!4u)I(4u,22;4u,22;T)$$
$$+2C(5g:{}^1\!4u,{}^1\!4u)C(5g:{}^2\!4u,{}^2\!4u)$$
$$\times I(4u,12;4u,12;T)+2C^2(5g:{}^1\!4u,{}^2\!4u)$$
$$\times[I(4u,12;4u,12;T)+I(4u,11;4u,22;T)]$$
$$+4C(5g:{}^1\!4u,{}^1\!4u)C(5g:{}^1\!4u,{}^2\!4u)$$
$$\times I(4u,11;4u,12;T)+4C(5g:{}^2\!4u,{}^2\!4u)$$
$$\times C(5g:{}^1\!4u,{}^2\!4u)I(4u,22;4u,12;T)$$
$$+2C^2(5g:{}^1\!4u,5u)I(4u,11;5u;T)$$
$$+2C^2(5g:{}^2\!4u,5u)I(4u,22;5u;T)$$
$$+4C(5g:{}^1\!4u,5u)C(5g:{}^2\!4u,5u)I(4u,12;5u;T)\ . \qquad (37)$$

The integrals $I(\beta,nn'';\gamma,n'n'''\lambda;T)$ are already defined in Eq. (19). We now evaluate these integrals in the perfect MgO lattice.

A. Phonon Integrals in Perfect MgO Lattices

The general method of evaluating the imaginary part of the G functions has already been discussed in Sec. II. In this particular case, the coefficients $A({}^n\Gamma:s)$ were calculated[13] for 125 000 points in the Brillouin zone, using the MgO shell model of Peckham.[9] By making use of the point-group operations only 3142 points need be considered. The final I integrals were calculated from the evaluations of the integrand at 600 evenly spaced values of the frequency ω. Each integral has been calculated at temperatures varying from 30 to 200 °K, at intervals of 10 °K. Obviously, the optical and the acoustical phonon are all automatically included in these integrals. At low temperatures the contributions from the acoustical phonons predominate over those from the optical phonons, and at high temperatures the opposite is the case. In Fig. 1 we show the phonon integrals for some even-parity modes, and these are compared with the corresponding Debye integrals. The phonon integrals for the Debye model can be evaluated from Eq. (A2). The eigenvectors $W_\alpha(k|\vec{k},p)$ in this equation satisfy the following orthogonality condition:

$$\sum_{k,\alpha} W_\alpha(k|\vec{k},p)W_\alpha(k|\vec{k},p')=\delta_{pp'}\ . \qquad (38)$$

If there are n atoms per unit cell and if the eigenvectors $\Phi_\alpha(k|\vec{k},p)$ associated with each of the atoms individually satisfy the orthogonality condition,[2] such that

$$\sum_{\alpha} \Phi_\alpha(k|\vec{k},p)\Phi_\alpha(k|\vec{k},p')=\delta_{pp'}\ , \qquad (39)$$

then, in terms of the Φ's we can rewrite Eq. (A2) as follows:

$$u_\alpha(l,k)=\sum_{\vec{k}}^{N/2}\sum_{p}\left(\frac{2}{Nnm_k}\right)^{1/2}\Phi_\alpha(k|\vec{k},p)$$
$$\times[q_1(\vec{k},p)\cos 2\pi\vec{k}\cdot\vec{x}(l,k)$$
$$-q_2(\vec{k},p)\sin 2\pi\vec{k}\cdot\vec{x}(l,k)]\ . \qquad (40)$$

Following Van Vleck[2] we also assume that all the ions have the same mass, so that we write,

$$u_\alpha(l,k)=\sum_{\vec{k}}^{N/2}\sum_{p}\left(\frac{2}{M}\right)^{1/2}\Phi_\alpha(k|\vec{k},p)$$
$$\times[q_1(\vec{k},p)\cos 2\pi\vec{k}\cdot\vec{x}(l,k)$$
$$-q_2(\vec{k},p)\sin 2\pi\vec{k}\cdot\vec{x}(l,k)]\ , \qquad (41)$$

where M is the mass of the crystal. Thus we get

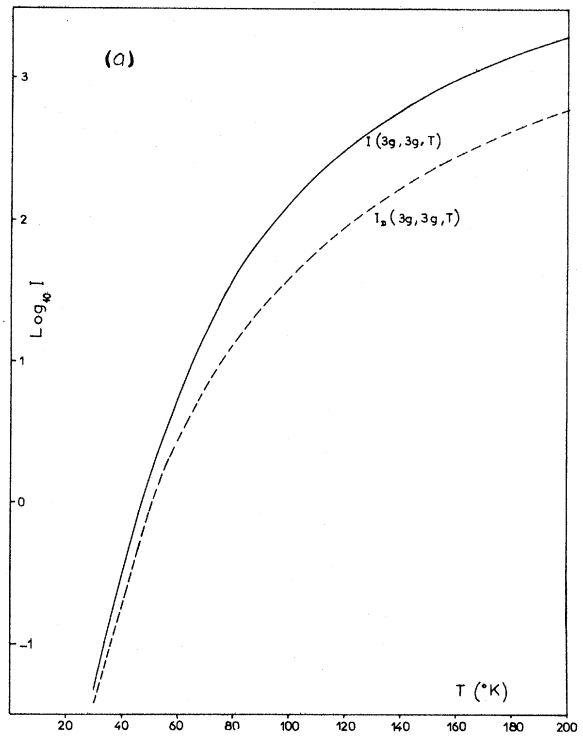

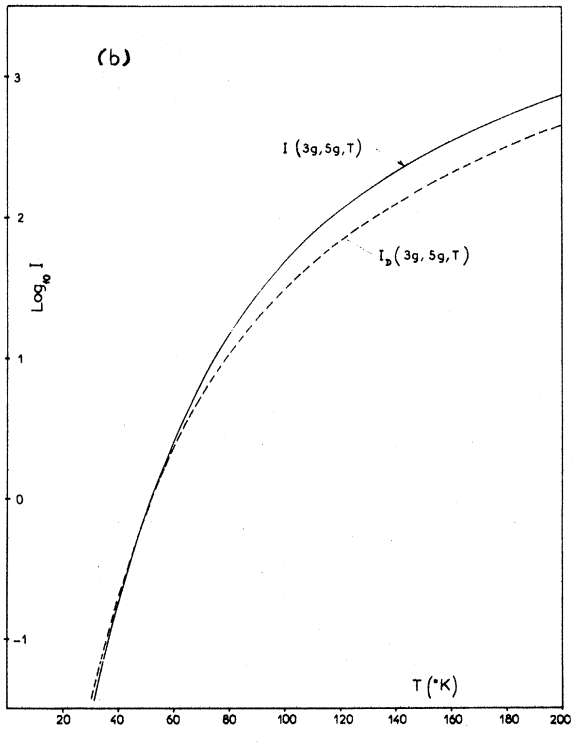

FIG. 1. (a) Plot of $\log_{10} I(3g, 3g, T)$ for the real phonon model (solid line) and the Debye model of phonons (dashed line) as a function of temperature in MgO crystal; (b) plot of $\log_{10} I(3g, 5g, T)$ for the real phonon model (solid line) and the Debye model of phonons (dashed line) as a function of temperature in MgO crystal.

$$A({}^n\Gamma_\beta^j{:}\, s) = -\sum_{\alpha,l,k}\left(\frac{2}{M}\right)^{1/2} A({}^n\Gamma_\beta^j{:}\, lk\alpha) \times \Phi_\alpha(k\,|\,s)\sin 2\pi\vec{k}\cdot\vec{x}(l,k) \tag{42}$$

for even modes, and

$$A({}^n\Gamma_\beta^j{:}\, s) = \sum_{\alpha,l,k}\left(\frac{2}{M}\right)^{1/2} A({}^n\Gamma_\beta^j{:}\, lk\alpha) \times \Phi_\alpha(k\,|\,s)\cos 2\pi\vec{k}\cdot\vec{x}(l,k) \tag{43}$$

for odd modes.

These coefficients $A(\Gamma_\beta^j{:}\, s)$ are related to the a coefficients defined by Van Vleck in Eq. (9) of Ref. 2, by the following expression:

$$A({}^n\Gamma_\beta{:}\, S) = 2(M^{-1/2})a({}^n\Gamma_\beta{:}\, s)\ . \tag{44}$$

For the Debye model, the Brillouin zone is a sphere, and consequently from Eq. (13) we have

$$R_{\Gamma_\beta}^{nn'}(s)(\text{Debye}) = \sum_{\substack{\text{spherical}\\ \text{average}}} A({}^n\Gamma_\beta{:}\, s)A({}^{n'}\Gamma_\beta{:}\, s) = \frac{2}{\pi^2\rho}\sum_p \frac{\omega^2}{v_p^3}\left\langle a\left({}^n\Gamma_\beta{:}\frac{\omega}{v_p}\right) a\left({}^{n'}\Gamma_\beta{:}\frac{\omega}{v_p}\right)\right\rangle_{\text{av}}\ ; \tag{45}$$

ρ is the density of the crystal and v_p is the velocity of Debye waves for polarization p. Therefore, Eq. (17) reduces to

$$\text{Im}G_\Gamma^{nn'}(\omega) = -\frac{\omega}{\pi\rho}\sum_p \frac{1}{v_p^3}\left\langle a\left({}^n\Gamma_\beta{:}\frac{\omega}{v_p}\right) a\left({}^{n'}\Gamma_\beta{:}\frac{\omega}{v_p}\right)\right\rangle_{\text{av}}\ . \tag{46}$$

The phonon integral for the Debye model, corresponding to Eq. (19), is therefore given by,

$$I_D(\Gamma_\beta, \Gamma_\gamma, T) = \frac{R^4}{\pi^2\rho^2 v_t^{10}}\sum\{I_6(\beta,\gamma,LL)\epsilon^{-10} + 4I_6(\beta,\gamma,TT) + 2\epsilon^{-5}[I_6(\beta,\gamma,LT) + I_6(\beta,\gamma,TL)]\}\ , \tag{47}$$

where[10]

$$I_n(\alpha,\beta,pp') = \int^{\omega_{\max}} \frac{\omega_{kp}^n \exp(\hbar\omega_{kp}/KT)}{[\exp(\hbar\omega_{kp}/KT)-1]^2}\left\langle\left(\frac{a(\Gamma_\alpha, kp)}{kR}\right)^2\right\rangle_{\text{av}} \times \left\langle\left(\frac{a(\Gamma_\beta, k'p')}{k'R}\right)^2\right\rangle_{\text{av}} d\omega\ \delta_{k',kv_p/v_{p'}}\ , \tag{48}$$

and where R is the nearest interatomic distance and $\epsilon = v_l/v_t$; with v_l and v_t being the Debye velocities for the longitudinal and transverse phonons, respectively. The I_n integrals were calculated[11] for β and γ corresponding to Γ_{1g}, Γ_{3g}, and Γ_{5g} modes with all different combinations of p and p'. In Fig. 1, we show the $I_D(3g{:}\,3g{:}\,T)$ and $I_D(3g{:}\,5g{:}\,T)$ for comparison with the corresponding real phonon integrals. As expected, the phonon integrals corresponding to the Debye model and the real phonon model agree very well in the low-temperature region, and they deviate from one another as the

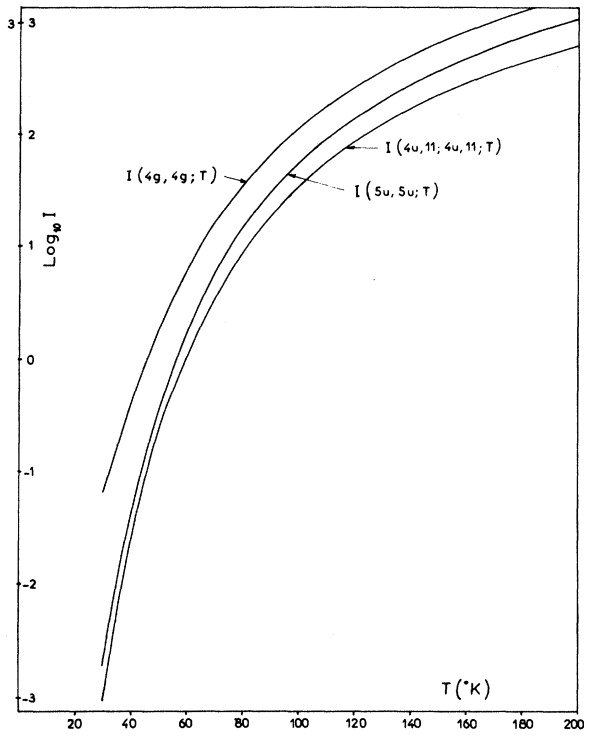

FIG. 2. Plots of $\log_{10}I(4g, 3g, T)$, $\log_{10}I(4u, 11; 4u, 11, T)$, and $\log_{10}(5u, 5u; T)$ for the real phonon model in MgO crystal as functions of temperature.

temperature increases. In Fig. 2, we have plotted some phonon integrals for the real phonon model for the rotational and the odd-parity representations. It is interesting to note that the phonon integrals for the odd-parity phonons are quite important, particularly in the high-temperature region. This indicates that the u modes which make no contribution in the long-wavelength limit, are as important as the even-parity modes in the Raman relaxation.

B. Evaluation of Orbit-Lattice Parameters in the XY_6 Complex

The six neighboring oxygen atoms around the embedded paramagnetic ion in the MgO lattice form an XY_6 complex. It is the effect of these immediate neighbors which is most important in the two phonon relaxation processes. We have assumed a point-charge model for the ligand ions because our interest in the present investigation lies in understanding the importance of the particular phonon model on the relaxation effects; and we try to see how far the choice of the phonon model itself can explain the available relaxation time data. We choose our nomenclature such that the paramagnetic ion is at the origin of the coordinate system and the oxygen atoms numbered $i (i = 1, 2, 3)$ are, respectively, on the x, y, and z axes and those numbered $i+3$ are, respectively, on the opposite sides of the central atom. In the present work, we assume no change in the lattice properties due to the substitution of the impurity ions. To evaluate the orbit-lattice parameters in this complex, we shall use Eqs. (26) and (27) and hence we need the symmetry-adapted displacements $Q(\Gamma^i_\alpha)$, the spherical harmonics $Y_l(\Gamma^i_\alpha)$, and the crystal field CG coefficients $\langle \Gamma^i_\alpha | \Gamma^j_\beta, \Gamma^l_\gamma \rangle$. The symmetry-adapted displacements in the XY_6 complex – of both odd and even parity – are listed in Table I. The ${}^3\Gamma_3 u$ displacements represent the pure translation of the complex and, hence, these particular displacements are of no consequence in the present calculations. The spherical harmonics which are necessary for our calculations are also given in Table I. It should be noted that l is restricted to the values 2 and 4 for the iron-group ions with d configuration. The odd-parity spherical harmonics corresponding to $l = 1$ and 3 are not considered, because we neglect the configuration mixing between the d and the p electrons. In Table II, we give the coefficients $A_{l,\alpha}$ which are calculated using Eq. (26). The Clebsch-Gordan coefficients in O_h symmetry that are used in Eq. (27) to evaluate $A_{l,\alpha,\beta,\gamma}$ are available in Ref. 15. The orbit-lattice parameters $A_{l,\alpha,\beta,\gamma}$ are tabulated in Table III. It should be noted that for the rotation-type Γ_{4g} displacements, the orbit-lattice interaction parameters are nonvanishing[14] and, consequently, these displacements contribute to the relaxation processes. In Table III, the $A_{l,\alpha,\beta,\gamma}$'s are tabulated only for $\alpha = 3g$ and $5g$, because the term corresponding to $\alpha = 4g$ will not cause any spin-phonon coupling for the ions $S < 2$. It should be mentioned that in Ref. 11 where the relaxation rates were calculated with the Debye model of phonons, all the constants $A_{l,\alpha}$ were already quoted. Of the $A_{l,\alpha,\beta,\gamma}$'s, however, only those corresponding to the even modes of displacements were calculated. One will notice a difference between these values and the corresponding values in Table III, the latter being less by a factor of $\frac{1}{2}$, which is due to an error in the previous calculations.

C. Evaluation of Spin-Phonon Coupling Parameters for Ni^{3+} and Cr^{3+} in MgO Crystals

To proceed with the calculations of the perturbations caused by the spin-orbit and orbit-lattice interactions, we define the crystal field states for Ni^{2+} and Cr^{3+} in O_h symmetry. Assuming no mixing between the F and the P states, the low-lying energy levels for these ions are as follows:

$$\psi({}^n\Gamma_{2g}) = (1/\sqrt{2}i)(|32\rangle - |3-2\rangle),$$

$$\psi({}^n\Gamma^1_{5g}) = (1/\sqrt{2})(|32\rangle + |3-2\rangle),$$

TABLE I. Symmetry-adapted displacements $Q(\Gamma_\alpha^i)$ in XY_6 symmetry and the corresponding spherical harmonics.

Representation Γ_α^i	Symmetry-adapted displacements $Q(\Gamma_\alpha^i)$	Spherical harmonic $Y_l(\Gamma_\alpha^i)$ $(l=2,4)$
Γ_{1g}^1	$6^{-1/2}(x_1-x_4+y_2-y_5+z_3-z_6)$	$(\frac{7}{12})^{1/2}[Y_4^0+(\frac{5}{12})^{1/2}(Y_4^4+Y_4^{-4})]$
Γ_{3g}^1	$3^{-1/2}[\frac{1}{2}(x_4-x_1+y_5-y_2)+(z_3-z_6)]$	Y_2^0, $(\frac{7}{6})^{1/2}[(\frac{5}{14})^{1/2}Y_4^0-\frac{1}{2}(Y_4^4+Y_4^{-4})]$
Γ_{3g}^2	$\frac{1}{2}[(x_1-x_4)+(y_5-y_2)]$	$(\frac{1}{2})^{1/2}(Y_2^2+Y_2^{-2})$, $-(\frac{1}{2})^{1/2}(Y_4^2+Y_4^{-3})]$
Γ_{4g}^1	$\frac{1}{2}(y_6-y_3+z_2-z_5)$	$-i(\frac{1}{2})^{1/2}[(\frac{7}{8})^{1/2}(Y_4^{-1}+Y_4^1)+(\frac{1}{8})^{1/2}(Y_4^3+Y_4^{-3})]$
Γ_{4g}^2	$\frac{1}{2}(x_3-x_6+z_4-z_1)$	$(\frac{1}{2})^{1/2}[(\frac{7}{8})^{1/2}(Y_4^{-1}-Y_4^1)+(\frac{1}{8})^{1/2}(Y_4^3-Y_4^{-3})]$
Γ_{4g}^3	$\frac{1}{2}(x_5-x_2+y_1-y_4)$	$-i(\frac{1}{2})^{1/2}(Y_4^4-Y_4^{-4})$
${}^1\Gamma_{4u}^1$	$6^{-1/2}(-2x_0+x_1+x_4)$	
${}^1\Gamma_{4u}^2$	$6^{-1/2}(-2y_0+y_2+y_5)$	
${}^1\Gamma_{4u}^3$	$6^{-1/2}(-2z_0+z_3+z_6)$	
${}^2\Gamma_{4u}^1$	$21^{-1/2}[2x_0-\frac{3}{2}(x_2+x_3+x_5+x_6)+2(x_1+x_4)]$	
${}^2\Gamma_{4u}^2$	$21^{-1/2}[2y_0-\frac{3}{2}(y_1+y_3+y_4+y_6)+2(y_2+y_5)]$	
${}^2\Gamma_{4u}^3$	$(21)^{-1/2}[2z_0-\frac{3}{2}(z_1+z_2+z_4+z_5)+2(z_3+z_6)]$	
${}^3\Gamma_{4u}^1$	$7^{-1/2}(x_0+x_1+x_2+x_3+x_4+x_5+x_6)$	
${}^3\Gamma_{4u}^2$	$7^{-1/2}(y_0+y_1+y_2+y_3+y_4+y_5+y_6)$	
${}^3\Gamma_{4u}^3$	$7^{-1/2}(z_0+z_1+z_2+z_3+z_4+z_5+z_6)$	
Γ_{5g}^1	$\frac{1}{2}(x_2-x_5+y_1-y_4)$	$i(2)^{-1/2}(Y_2^2-Y_2^{-2})$; $-i(2)^{-1/2}(Y_4^2-Y_4^{-2})$
Γ_{5g}^2	$\frac{1}{2}(x_3-x_6+z_1-z_4)$	$-2^{-1/2}(Y_2^1-Y_2^{-1})$; $(\frac{1}{2})^{1/2}(\frac{7}{8})^{1/2}(Y_4^{-3}-Y_4^3)+(\frac{1}{8})^{1/2}(Y_4^{-1}-Y_4^1)]$
Γ_{5g}^3	$\frac{1}{2}(y_3-y_6+z_2-z_5)$	$i2^{-1/2}(Y_2^1+Y_2^{-1})$, $i(2)^{-1/2}[(\frac{7}{8})^{1/2}(Y_4^{-3}+Y_4^3)-(\frac{1}{8})^{1/2}(Y_4^1+Y_4^{-1})]$
Γ_{5u}^1	$\frac{1}{2}(x_2-x_3+x_5-x_6)$	
Γ_{5u}^2	$\frac{1}{2}(y_3-y_1+y_6-y_4)$	
Γ_{5u}^3	$\frac{1}{2}(z_1-z_2+z_4-z_5)$	

$$\psi({}^n\Gamma_{5g}^2)=\tfrac{1}{4}i[\sqrt{5}(|31\rangle+|3-1\rangle)-\sqrt{3}(|33\rangle+|3-3\rangle)],$$
$$\psi({}^n\Gamma_{5g}^3)=\tfrac{1}{4}[\sqrt{5}(|31\rangle-|3-1\rangle)+\sqrt{3}(|33\rangle-|3-3\rangle)],$$
$$\psi({}^n\Gamma_{4g}^1)=-\tfrac{1}{4}[\sqrt{3}(|31\rangle-|3-1\rangle)-\sqrt{5}(|33\rangle-|3-3\rangle)],$$
$$\psi({}^n\Gamma_{4g}^2)=\tfrac{1}{4}i[\sqrt{3}(|31\rangle+|3-1\rangle)+\sqrt{5}(|33\rangle+|3-3\rangle)],$$
$$\psi({}^n\Gamma_{4g}^3)=-|30\rangle\ , \qquad (49)$$

where n is 3 for Ni^{2+} and 4 for Cr^{3+}.

Of these, Γ_{2g} is the ground level with Γ_{5g} and Γ_{4g} lying at energy separation Δ_1 and Δ_2, respectively, above it. (In the present calculations, the excited ${}^2\Gamma_{3g}$-orbital levels need not be considered because these levels are not connected to the ground Γ_{2g} levels through the orbit-lattice interaction and, thus, they do not contribute to the spin-phonon coupling parameters.) Then with the quadratic part of $\mathcal{H}_{o-l}$, we calculate the third-order change in the ground-state energy $\Delta E^{(3)}$ as given by Eq. (28), and compare this, term by term, with the expression of the dynamical Hamiltonian in O_h symmetry to get the "third-order contribution" to the spin-phonon coupling parameters $C(\alpha:n\beta,n'\gamma)$. Similarly, with the linear term of $\mathcal{H}_{o-l}$ we calculate the fourth-order change in the energy, namely, $\Delta E^{(4)}$ as given by Eq. (15) and compare the expression of the energy with that of the dynamical Hamiltonian so that we obtain the "fourth-order contributions" to the spin-phonon coupling parameters which are associated with even parity Q. In Table IV, we give the algebraic expressions of the spin-phonon coupling coefficients, and the numerical values of these constants are tabulated in Table V for Ni^{2+} and Cr^{3+} ions in MgO. The numbers are calculated with the following values of the different parameters.

For Ni^{2+}, [16,17]

TABLE II. The first-order orbit-lattice parameters $A_{l,\alpha}$ in the XY_6 complex.

l	α	$A_{l,\alpha}(\sqrt{\pi}Ze^2/R^4)^{-1}$
2	$3g$	$6(\frac{3}{5})^{1/2}$
	$5g$	$-4(\frac{3}{5})^{1/2}$
4	$3g$	$5(5)^{1/2}/3R^2$
	$4g$	$-2(\sqrt{35})^{1/2}/3R^2$
	$5g$	$-2(5)^{1/2}/3R^2$

TABLE III. Second-order orbit-lattice parameters $A_{l,\alpha,\beta,\gamma}$ in the XY_6 complex for $\alpha = 3g$ and $5g$.

α	β	γ	$A_{l,\alpha,\beta,\gamma}(\sqrt{\pi}Ze^2/R^n)^{-1}$ $l=2$, $n=5$	$l=4$, $n=7$
$3g$	$1g$	$3g$	$-\frac{6\sqrt{2}}{\sqrt{5}}$	$-\frac{5\sqrt{5}}{\sqrt{6}}$
	$3g$	$3g$	$-\frac{6\sqrt{2}}{\sqrt{5}}$	$-\frac{5\sqrt{5}}{\sqrt{6}}$
	$4g$	$4g$	$\frac{3\sqrt{3}}{2\sqrt{10}}$	$\frac{11\sqrt{5}}{4\sqrt{2}}$
	$4g$	$5g$	$-\frac{21}{2\sqrt{10}}$	$-\frac{3\sqrt{15}}{4\sqrt{2}}$
	$5g$	$5g$	$\frac{3\sqrt{3}}{2\sqrt{10}}$	$\frac{11\sqrt{5}}{4\sqrt{2}}$
	$^1 4u$	$^2 4u$	$\frac{24\sqrt{6}}{\sqrt{5}}$	$\frac{43\sqrt{5}}{3\sqrt{2}}$
	$^1 4u$	$^2 4u$	$-\frac{3\sqrt{21}}{\sqrt{5}}$	$\frac{\sqrt{35}}{6}$
	$^1 4u$	$5u$	$-\sqrt{15}$	$-\frac{7\sqrt{5}}{2}$
	$^2 4u$	$^2 4u$	$\frac{21\sqrt{3}}{2\sqrt{10}}$	$-\frac{7\sqrt{5}}{12\sqrt{2}}$
	$^2 4u$	$5u$	$\frac{\sqrt{105}}{2\sqrt{2}}$	$\frac{7\sqrt{35}}{4\sqrt{2}}$
	$5u$	$5u$	$\frac{9\sqrt{6}}{2\sqrt{5}}$	$-\frac{\sqrt{5}}{4\sqrt{2}}$
$5g$	$1g$	$5g$	$\frac{4\sqrt{2}}{\sqrt{5}}$	$\frac{\sqrt{10}}{\sqrt{3}}$
	$3g$	$4g$	$-\frac{4\sqrt{3}}{\sqrt{5}}$	$-\sqrt{5}$
	$3g$	$5g$	$\frac{4}{\sqrt{5}}$	$\frac{\sqrt{5}}{\sqrt{3}}$
	$4g$	$4g$	$\frac{\sqrt{3}}{\sqrt{10}}$	$-\frac{\sqrt{10}}{2}$
	$4g$	$5g$	$-\frac{\sqrt{3}}{\sqrt{10}}$	$\frac{\sqrt{10}}{2}$
	$5g$	$5g$	$-\frac{\sqrt{3}}{\sqrt{10}}$	$\frac{\sqrt{10}}{2}$
	$^1 4u$	$^1 4u$	$\frac{44\sqrt{2}}{\sqrt{15}}$	$\frac{32\sqrt{5}}{3\sqrt{2}}$
	$^1 4u$	$^2 4u$	$-\frac{10\sqrt{7}}{\sqrt{15}}$	$-\frac{5\sqrt{35}}{3}$
	$^2 4u$	$^2 4u$	$-\frac{7}{\sqrt{30}}$	$\frac{7\sqrt{5}}{3\sqrt{2}}$
	$^1 4u$	$5u$	$\frac{14}{\sqrt{5}}$	$\frac{\sqrt{5}}{\sqrt{3}}$
	$^2 4u$	$5u$	$-\frac{\sqrt{7}}{\sqrt{10}}$	$\frac{\sqrt{35}}{\sqrt{6}}$
	$5u$	$5u$	$\frac{\sqrt{3}}{\sqrt{10}}$	$-\frac{\sqrt{10}}{2}$

$\Delta_1 = 8.600\,\mathrm{cm}^{-1}$, $\Delta_2 = \frac{9}{5}\Delta_1$,

$\langle r_0^2 \rangle = 1.13$ a.u., $\langle r_0^4 \rangle = 33.003$ a.u.,

$\lambda = -245\,\mathrm{cm}^{-1}$, and $Z_{eff} = -7.72$; (50)

and for Cr^{3+}, [17,18]

$\Delta_1 = 22\,700\,\mathrm{cm}^{-1}$, $\Delta_2 = \frac{9}{5}\Delta_1$,

$\langle r_0^2 \rangle = 1.447$ a.u., $\langle r_0^4 \rangle = 4.297$ a.u,

$\lambda = 63\,\mathrm{cm}^{-1}$, and $Z_{eff} = -14.2$. (51)

The Z_{eff} for Ni^{2+} and Cr^{3+} were evaluated by comparing the theoretical and experimental values of the static crystal field splitting of the ground term. By this we assume the covalency and overlap effects in the dynamical problem to be of the same order as those in the static case.

D. Relaxation Rates of Ni^{2+} and Cr^{3+} in MgO Crystals

Knowing the phonon integrals I and the spin-phonon coupling coefficients C, the summations S_{1g}, S_{2g}, S_{1u}, and S_{2u} given by Eqs. (34)–(37), respectively, are numerically evaluated as functions of temperature from 30 to 200 °K for Ni^{2+} and Cr^{3+} ions. The relative importance of the phonon integrals in these summations will be determined by the magnitude of the associated spin-phonon coupling coefficient.

1. *Case of* Ni^{2+}

For the single-spin transition

$$W_1 = W_{1\to 0} = (2/\pi)[(S_{1g}+S_{1u})+(l^4+m^4+n^4)(-S_{1g}-S_{1u}+S_{2g}+S_{2u})], \quad (52)$$

and for the double-spin transition,

$$W_2 = W_{-1\to 1} = \pi^{-1}[(S_{1g}+S_{1u}+3S_{2g}+3S_{2u})+(l^4+m^4+n^4) \times (S_{1g}+S_{1u}-S_{2g}-S_{2u})] \ . \quad (53)$$

If we write f for the angular factor $l^4+m^4+n^4$, then for the Zeeman field along one of the crystal axes $\langle 100 \rangle$ we have $f=1$ and the corresponding values of W_1 and W_2 are

$$(W_1)_{f=1} = (2/\pi)(S_{2g}+S_{2u}) \ , \quad (54)$$

$$(W_2)_{f=1} = (2/\pi)(S_{1g}+S_{1u}+S_{2g}+S_{2u}) \ . \quad (55)$$

For H along the [111] direction, $f=\frac{1}{3}$ and the corresponding values of W_1 and W_2 are

$$(W_1)_{f=1/3} = (2/3\pi)(2S_{1g}+2S_{1u}+S_{2g}+S_{2u}) \ , \quad (56)$$

$$(W_2)_{f=1/3} = (4/3\pi)(S_{1g}+S_{1u}+2S_{2g}+2S_{2u}) \ . \quad (57)$$

Thus, though the Zeeman energy is independent of the crystal orientation, the relaxation rates are not because the orbit-lattice interaction, being dependent on the nature of the displacement of the ligand ions, is anisotropic. For Ni^{2+}, there are two possible relaxation rates (i) $1/T_1 = W_1 + 2W_2$ and (ii) $1/T_1 = 3W_1$. In Table IV, we have given the maximum and minimum values of these relaxation rates at 50, 100, and 150 °K for the real phonon model. The relaxation rate $1/T_1 = W_1 + 2W_2$ does not show any anisotropy as the angular factor

TABLE IV. Expressions for the spin-phonon coupling coefficients for Ni^{2+} and Cr^{3+} ions in O_h symmetry: $a_1 = Ze^2/R^4\langle r^2\rangle$; $a_2 = Ze^2/R^6\langle r^4\rangle$; $e_1 = \lambda^2/\Delta_1^2$; $e_2 = \lambda^2/\Delta_2^2$; $x_1 = e_1a_1/R$; $x_2 = e_1a_2/R$; $y_1 = 1 + 2\Delta_1/\Delta_2$; and $y_2 = -2 + 3\Delta_1/\Delta_2$.

$C(\alpha:n\beta, n'\gamma)$	Third-order contribution (x)	Fourth-order contribution (y)
$C(3g:1g, 3g)$	$\frac{25}{\sqrt{3}}x_2$	$\frac{1250\sqrt{3}}{27}\frac{e_1a_2^2}{\Delta_1}$
$C(3g:3g, 3g)$	$\frac{25}{\sqrt{3}}x_2$	$\frac{-625\sqrt{3}}{54}\frac{e_1a_2^2}{\Delta_1}+\frac{\sqrt{3}}{1470}\frac{e_1}{\Delta_2}(36a_1+25a_2)^2$
$C(3g:4g, 4g)$	$-\frac{55}{4}x_2$	$-\frac{5}{36}e_1a_2^2\left(\frac{5}{\Delta_1}+\frac{243}{\Delta_2}\right)$
$C(3g:4g, 5g)$	$\frac{15\sqrt{3}}{4}x_2$	$\frac{10}{21\sqrt{3}}\frac{e_1a_2}{\Delta_1}(9a_1-5a_2)+\frac{18}{7\sqrt{3}}\frac{e_1a_2}{\Delta_2}(3a_1+10a_2)+\frac{27}{14\sqrt{3}}\frac{e_2a_2}{\Delta_1}$ $\times(12a_1+5a_2)+\frac{5}{14\sqrt{3}}\frac{e_1a_2}{\Delta_2}(12a_1+5a_2)$
$C(3g:5g, 5g)$	$-\frac{55}{4}x_2$	$-\frac{4}{441}\frac{e_1}{\Delta_1}(9a_1-5a_2)^2-\frac{2}{147}\frac{e_1}{\Delta_2}[(9a_1-5a_2)(12a_1+5a_2)$ $+\frac{2}{5}(3a_1+10a_2)^2]-\frac{e_2}{49\Delta_1}(12a_1+5a_2)[\frac{2}{5}(3a_1+10a_2)$ $+\frac{1}{4}(12a_1+5a_2)]-\frac{3}{980}\frac{e_2}{\Delta_2}(12a_1+5a_2)^2$
$C(3g:{}^14u, {}^14u)$	$-\frac{215}{3}x_2$	
$C(3g:{}^14u, {}^24u)$	$-\frac{5\sqrt{14}}{6}x_2$	
$C(3g:{}^14u, 5u)$	$\frac{35}{\sqrt{2}}x_2$	
$C(3g:{}^24u, {}^24u)$	$\frac{35}{12}x_2$	
$C(3g:{}^24u, 5u)$	$-\frac{35\sqrt{7}}{4}x_2$	
$C(3g:5u, 5u)$	$\frac{5}{4}x_2$	
$C(5g:1g, 5g)$	$\frac{8\sqrt{3}}{7}x_1y_1+\frac{10}{7\sqrt{3}}x_2y_2$	$\frac{200}{63\sqrt{3}}\frac{e_1}{\Delta_1}a_2(9a_1-5a_2)+\frac{10}{21\sqrt{3}}\left(\frac{5e_1}{\Delta_2}+\frac{9e_2}{\Delta_1}\right)(12a_1+5a_2)a_2$
$C(5g:3g, 4g)$	$-\frac{12\sqrt{2}}{7}x_1y_1-\frac{5\sqrt{2}}{7}x_2y_2$	$-\frac{125}{9\sqrt{2}}\frac{e_1}{\Delta_1}a_2^2-\frac{19}{21\sqrt{2}}\frac{e_1}{\Delta_2}a_2(36a_1+25a_2)$
$C(5g:3g, 5g)$	$\frac{4\sqrt{6}}{7}x_1y_1+\frac{5\sqrt{2}}{7\sqrt{3}}x_2y_2$	$-\frac{100}{63\sqrt{6}}\frac{e_1a_2}{\Delta_1}(9a_1-5a_2)-\frac{20}{7\sqrt{6}}\left(\frac{5}{12}a_2(12a_1+5a_2)-\frac{1}{175}\right.$ $\left.\times(36a_1+25a_2)(3a_1+10a_2)\right)\frac{e_1}{\Delta_2}+\frac{e_2}{245\sqrt{6}\Delta_1}(12a_1+5a_2)$ $\times(252a_1-175a_2)$
$C(5g:4g, 4g)$	$\frac{3}{7}x_1y_1-\frac{5}{7}x_2y_2$	$\frac{5}{18}e_1a_2^2\left(\frac{5}{2}\frac{1}{\Delta_1}-\frac{3}{2}\frac{1}{\Delta_2}\right)$
$C(5g:4g, 5g)$	$-\frac{3}{7}x_1y_1+\frac{5}{7}x_2y_2$	$\frac{10}{63}\frac{e_1}{\Delta_1}a_2(9a_1-5a_2)+\frac{2}{21}\frac{e_1}{\Delta_2}a_2(3a_1+10a_2)$ $-\frac{e_2}{\Delta_1}a_2(12a_1+5a_2)$
$C(5g:5g, 5g)$	$-\frac{3}{7}x_1y_1+\frac{5}{7}x_2y_2$	$-\frac{4}{441}\frac{e_1}{\Delta_1}(9a_1-5a_2)^2+\frac{3}{980}\frac{e_2}{\Delta_2}(12a_1+5a_2)^2-\frac{2}{147}\frac{e_1}{\Delta_2}$ $\times\left\{(9a_1-5a_2)(12a_1+5a_2)-\frac{2}{5}(3a_1+10a_2)^2\right\}+\frac{1}{49}\frac{e_2}{\Delta_1}$ $\times(12a_1+5a_2)\left\{-\frac{4}{5}(3a_1-25a_2)+\frac{2}{5}(3a_1+10a_2)\right.$ $\left.-\frac{1}{4}(12a_1+5a_2)\right\}$

TABLE IV. (*Continued*)

$C(\alpha:n\beta, n'\gamma)$	Third-order contribution (x)	Fourth-order contribution (y)
$C(5g:{}^1\!4u, {}^1\!4u)$	$\frac{88}{7}x_1y_1+\frac{160}{21}x_2y_2$	
$C(5g:{}^1\!4u, {}^2\!4u)$	$-\frac{10\sqrt{2}}{\sqrt{7}}x_1y_1-\frac{25\sqrt{2}}{3\sqrt{7}}x_2y_2$	
$C(5g:{}^1\!4u, 5u)$	$2\sqrt{6}\,x_1y_1+\frac{5\sqrt{2}}{7\sqrt{3}}x_2y_2$	
$C(5g:{}^2\!4u, {}^2\!4u)$	$-x_1y_1+\frac{5}{3}x_2y_2$	
$C(5g:{}^2\!4u, 5u)$	$-\frac{\sqrt{3}}{\sqrt{7}}x_1y_1+\frac{5}{\sqrt{21}}x_2y_2$	
$C(5g:5u, 5u)$	$\frac{3}{7}x_1y_1-\frac{5}{7}x_2y_2$	

exactly cancels. The other relaxation rate is maximum for $\vec{H}\|\langle 100\rangle$ directions and minimum for $\vec{H}\|\langle 111\rangle$ directions. The results given in Table VI indicate that the contributions of the u modes increase with temperature more than those of the g modes. Comparison of the results obtained from the real phonon model for $1/T_1 = 3W_1$ with $\vec{H}\|\langle 111\rangle$ directions with those calculated from the Debye model is made in Fig. 3. In the Debye model, the usual long-wavelength approximation has to be made because the phonon response functions for the odd-parity and the rotational Γ_{4g} modes have not yet been worked out for the Debye model at any arbitrary frequency ω. In the long-wavelength limit we have $\langle[a(\Gamma^i_{4g}, \vec{k}p)]^2/k^2R^2\rangle_{\rm av}=0$ for the longitudinal Γ_{4g} mode and $\langle[a(\Gamma^i_{4g}, \vec{k}p)]^2/k^2R^2\rangle_{\rm av}=\frac{1}{6}$ for the transverse Γ_{4g} modes. The odd-parity modes contribute very little to relaxation rates in the long-wavelength approximation. From Eq. (47) and using the long-wavelength approximation, we get the following expression for W_1 for $H\|\langle 111\rangle$ direction:

$$W_1=\frac{64R^4}{3\pi^3\rho^2 v_t^{10}}\left(\frac{k}{\hbar}\right)^7\{\{[C(5g:1g,5g)]^2 + 2[C(3g:1g,3g)]^2\}(1+\tfrac{3}{2}\epsilon^5) + \tfrac{2}{5}\{[C(5g:3g,5g)]^2+[C(5g:5g,5g)]^2 + 2[C(3g:3g,3g)]^2+2[C(3g:5g,5g)]^2\}(1+\tfrac{3}{2}\epsilon^5)^2 + \{[C(5g:3g,4g)]^2+[C(5g:4g,5g)]^2 + 2[C(3g:4g,5g)]^2\}(1+\tfrac{3}{2}\epsilon^5)\epsilon^5 + \tfrac{5}{2}\{[C(5g:4g,4g)]^2+2[C(3g:4g,4g)]^2\}\epsilon^{10})T^7. \quad (58)$$

TABLE V. Magnitudes of the spin-phonon coupling coefficients for Ni^{2+} and Cr^{3+} ions in MgO (in units of erg cm^{-2})

	Ni^{2+}			Cr^{3+}		
	Third order	Fourth order	Total	Third order	Fourth order	Total
$C(3g:1g,3g)$	−27.27	91.07	63.80	−0.68	2.27	1.59
$C(3g:3g,3g)$	−27.27	19.47	−7.81	−0.68	0.30	−0.38
$C(3g:4g,4g)$	25.98	−22.08	3.90	0.65	−0.55	0.10
$C(3g:4g,5g)$	−12.27	80.73	68.45	−0.31	1.83	1.52
$C(3g:5g,5g)$	25.98	−78.17	−52.19	0.65	−1.56	−0.91
$C(3g:{}^1\!4u, {}^1\!4u)$	135.42	0	135.20	3.38	0	3.38
$C(3g:{}^1\!4u, {}^2\!4u)$	5.89	0	5.89	0.15	0	0.15
$C(3g:{}^2\!4u, {}^2\!4u)$	−5.51	0	−5.51	−0.14	0	−0.14
$C(3g:{}^1\!4u, 5u)$	−46.77	0	−46.77	−1.17	0	−1.17
$C(3g:{}^2\!4u, 5u)$	43.74	0	43.74	1.09	0	1.09
$C(3g:5u, 5u)$	−2.36	0	−2.36	−0.06	0	−0.06
$C(5g:1g, 5g)$	−46.27	232.66	186.38	−1.03	5.18	4.15
$C(5g:3g, 4g)$	56.68	−107.37	−50.69	1.27	−2.45	−1.18
$C(5g:3g, 5g)$	−32.72	27.55	−5.18	−0.73	0.44	−0.29
$C(5g:4g, 4g)$	−10.58	0.53	−10.05	−0.24	0.01	−0.23
$C(5g:4g, 5g)$	10.58	−10.58	0.00	0.24	−0.24	0.00
$C(5g:5g, 5g)$	10.58	−49.55	−38.97	0.24	−0.97	−0.73
$C(5g:{}^1\!4u, {}^1\!4u)$	−292.38	0	−292.38	−6.52	0	−6.52
$C(5g:{}^1\!4u, {}^2\!4u)$	123.56	0	123.56	2.75	0	2.75
$C(5g:{}^1\!4u, 5u)$	−115.44	0	−115.44	−2.58	0	−2.58
$C(5g:{}^2\!4u, {}^2\!4u)$	24.69	0	24.69	0.55	0	0.55
$C(5g:{}^2\!4u, 5u)$	16.16	0	16.16	0.36	0	0.36
$C(5g:5u, 5u)$	−10.58	0	−10.58	−0.24	0	−0.24

As expected, Fig. 3 shows that the real phonon results and the Debye results do not differ much up to 100 °K. The relaxation time becomes too short above this temperature and can not therefore, be directly measured. But recently Smith, Dravnicks, and Wertz[10] have measured the relaxation rates for Ni^{2+} in MgO from the line-shape function at 123 and 136 °K for the Zeeman field along one of the body diagonals. By comparing our expression for W_1 with the parameter K_1 defined by Eq. (17) in Ref. 10 we get $(1/T_1)_{\rm expt}=3W_1=0.12\times10^8$ and 0.15×10^8 sec^{-1} at 123 and 136 °K, respectively. At these temperatures, the real phonon results give $1/T_1=0.15\times10^8$ and 0.23×10^8 sec^{-1}. The Debye results, on the other hand, are 0.16×10^8 and 0.36×10^8 sec^{-1}. Both, as regards the absolute magnitudes and the functional form of the dependence on temperature, the experimental values of $1/T_1$ are in better agreement with real phonon results than those obtained from the Debye model.

TABLE VI. Transition probabilities and relaxation rates for Ni^{2+} in MgO.

Temperature (°K)	S_{1g} (sec^{-1})	S_{2g} (sec^{-1})	S_{1u} (sec^{-1})	S_{2u} (sec^{-1})	Transition probability W_1(sec^{-1}) Max.	W_1 Min.	W_2(sec^{-1}) Max.	W_2 Min.	$1/T_1$(sec^{-1}) Max.	$1/T_1$ Min.
50	0.68164 ×10^4	0.10504 ×10^5	0.73519 ×10^4	0.51355 ×10^5	0.394 ×10^5	0.191 ×10^5	0.585 ×10^5	0.484 ×10^5	(i) 1.36 ×10^5	1.36 ×10^5
									(ii) 1.18 ×10^5	0.57 ×10^5
100	0.43236 ×10^6	0.96874 ×10^6	0.93856 ×10^6	0.51533 ×10^7	0.389 ×10^7	0.188 ×10^7	0.577 ×10^7	0.477 ×10^7	(i) 1.34 ×10^7	1.34 ×10^7
									(ii) 1.17 ×10^7	0.56 ×10^7
150	0.25771 ×10^7	0.65168 ×10^7	0.59297 ×10^7	0.29543 ×10^8	0.230 ×10^8	0.113 ×10^8	0.342 ×10^8	0.284 ×10^8	(i) 0.80 ×10^8	0.80 ×10^8
									(ii) 0.69 ×10^8	0.34 ×10^8

2. *Case of* Cr^{3+}

In this case, the single-spin transition probability is given by

$$W_1 = W_{1/2\to -1/2} = (12/\pi)[(S_{1g} + S_{1u}) + (l^4 + m^4 + n^4)(S_{2g} + S_{2u} - S_{1g} - S_{1u})]; \quad (59)$$

and for the double-spin transition, it is

$$W_2 = W_{-3/2\to 1/2} = (3/\pi)[(S_{1g} + S_{1u} + 3S_{2g} + 3S_{2u}) + (l^4 + m^4 + n^4)(S_{1g} + S_{1u} - S_{2g} - S_{2u})] . \quad (60)$$

For the Zeeman field along the [100] and [111] directions, the transition probabilities are, respectively,

$$(W_1)_{f=1} = (12/\pi)(S_{2g} + S_{2u}) , \quad (61)$$

$$(W_1)_{f=1/3} = (4/\pi)(2S_{1g} + 2S_{1u} + S_{2g} + S_{2u}) ,$$

and

$$(W_2)_{f=1} = (6/\pi)(S_{1g} + S_{1u} + S_{2g} + S_{2u}) , \quad (62)$$

$$(W_2)_{f=1/3} = (4/\pi)(S_{1g} + S_{1u} + 2S_{2g} + 2S_{2u}) .$$

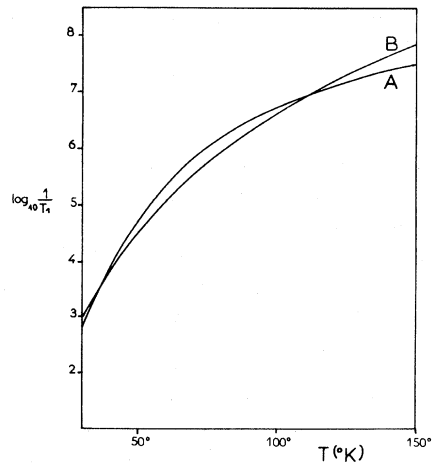

FIG. 3. Plots of $\log_{10}(1/T_1)$ versus T for Ni^{2+} in MgO: (T_1 in seconds) (a) real phonon results, and (b) Debye results.

In Table VII, the values of S_{1g}, S_{2g}, S_{1u}, S_{2u} and the corresponding maximum and minimum values of W_1 and W_2 are quoted at 60, 100, and 200 °K. The three possible relaxation rates (i) $1/T_1 = 2W_1$, (ii) $1/T_1 = 2W_2$, and (iii) $1/T_1 = 2W_1 + 2W_2$ are tabulated in the last column. That the relative contributions of the u modes are more important at higher temperature is evident from these results for Cr^{3+}. Unlike the Ni^{2+} case, here all three relaxation rates show some anisotropy. In Fig. 4 we compare the real phonon results with those obtained with the Debye model in the long-wavelength limit for the case of $1/T_1 = 2W_1$ and the Zeeman field along one of the crystal axes. Here also, the temperature dependence of the two sets of results differ appreciably above 100 °K. Experimentally, the relaxation rate of Cr^{3+} in MgO has been measured up to 200 °K and the results were fitted with the following empirical relation between 65 and 200 °K[7]:

$$1/T_1 = Ae^{\kappa_1}/(e^{\kappa_1} - 1)^2 + Be^{-\kappa_2} , \quad (63)$$

where $\kappa_1 T = 400$ °K, $\kappa_2 T = 700$ °K, $A = 3\times 10^6$ sec^{-1}, and $B/A = (4.5)^2$. In Fig. 4 we have plotted the experimental values of $1/T_1$ to compare these results with those given by the real phonon and Debye models. We have chosen arbitrarily one of the relaxation rates $1/T_1 = 2W_1$ for comparison with the experimental results, because the dependence on temperature appears to be nearly the same for all the three relaxation times. They are, also, of the same order of magnitude. On comparing the experimental results with those given by the real phonon model, we find that the ratio $(1/T_1)_{\text{expt}}/(1/T_1)_{\text{real phonon}}$ is fairly constant over the temperature range considered, the average value being 5.4. Thus, for Cr^{3+} in MgO also, the real phonon re-

TABLE VII. Transition probabilities and relaxation rates for Cr^{3+} in MgO.

Temperature (°K)	Transition Probability (sec^{-1}) S_{1g}	S_{2g}	S_{1u}	S_{2u}	$W_1(sec^{-1})$ Max.	W_1 Min.	$W_2(sec^{-1})$ Max.	W_2 Min.	$1/T_1(sec^{-1})$ Max.	$1/T_1$ Min.
60	0.112 91 $\times 10^2$	0.194 47 $\times 10^2$	0.209 57 $\times 10^2$	0.110 23 $\times 10^3$	0.495 $\times 10^3$	0.247 $\times 10^3$	0.371 $\times 10^3$	0.309 $\times 10^3$	(i) 0.99 $\times 10^3$ (ii) 0.74 $\times 10^3$ (iii) 1.73 $\times 10^3$	0.49 $\times 10^3$ 0.62 $\times 10^5$ 1.11 $\times 10^3$
100	0.225 42 $\times 10^3$	0.492 41 $\times 10^3$	0.585 61 $\times 10^3$	0.256 57 $\times 10^4$	0.117 $\times 10^5$	0.596 $\times 10^4$	0.882 $\times 10^4$	0.739 $\times 10^4$	(i) 0.23 $\times 10^5$ (ii) 1.76 $\times 10^4$ (iii)0.41 $\times 10^5$	1.19 $\times 10^4$ 1.48 $\times 10^4$ 0.27 $\times 10^5$
200	0.358 28 $\times 10^4$	0.934 81 $\times 10^4$	0.101 03 $\times 10^5$	0.385 89 $\times 10^5$	0.183 $\times 10^6$	0.959 $\times 10^5$	0.139 $\times 10^6$	0.118 $\times 10^6$	(i) 0.37 $\times 10^6$ (ii) 0.27 $\times 10^6$ (iii) 0.64 $\times 10^6$	1.92 $\times 10^5$ 0.24 $\times 10^6$ 0.43 $\times 10^6$

sults for $1/T_1$ show the same dependence on temperature as the experimental relaxation rates but unlike the Ni^{2+} case, the theoretical values are less than the experimental values by a factor of about 6.

V. DISCUSSION

There are three features of the spin-lattice relaxation time, namely, (i) the variation with temperature, (ii) the magnitude, and (iii) the anisotropy with respect to the orientation of the Zeeman field, which should be correctly accounted for by any theoretical model. In this paper we have studied these features for Ni^{2+} and Cr^{3+} in MgO, assuming a phonon model which gives an adequate account of the neutron scattering experiments on MgO crystal and, also, for the Debye model of phonons. For Ni^{2+}, the two sets of results – one for the assumed phonon model and the other for the Debye model – show the same order of variation with temperature up to 100 °K. Above 100 °K, the dependence on temperature of the relaxation rates is different for the two models. The values of $1/T_1$ at 123 and 136 °K obtained from the line-shape studies are the same as the theoretical values calculated assuming the real phonon model. In the effective point-change model, the value of Z_{eff} for Ni^{2+} in MgO is -7.72 for both the static and dynamic crystalline potential, which differs considerably from the free ionic value of -2. The overlap and covalency effects are found to increase the static crystal field parameters for both iron-group and rare-earth ions.[19] It will be interesting to see whether for Ni^{2+} in MgO, the overlap and covalency effects explain simultaneously the static and dynamic parameters, just as in the point-change model, where the same value of Z_{eff} has accounted for both the static and dynamic parameters. For the case of Cr^{3+}, direct measurements of $1/T_1$ have been done over the temperature region 65–200 °K. In order to compare the functional form of the tem-

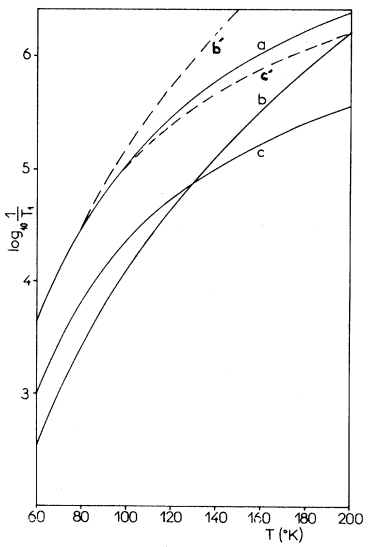

FIG. 4. Plots of $\log_{10}(1/T_1)$ versus T for Cr^{3+} in MgO: (T_1 in seconds) (a) the experimental curve, (b) the theoretical curve with the Debye model of phonons in the long wave length limit, and (c) the theoretical curve with the real model of phonons; (b′) and (c′) are the curves (b) and (c) superimposed on the curve (a).

perature dependence of $(1/T_1)_{expt}$ with those obtained from the real phonon and the Debye models, we have superimposed the two theoretical curves on the experimental one in Fig. 4. It is seen that the real phonon curve is in good agreement with the experimental one, though small discrepancies appear in the high-temperature region. The expressions for $1/T_1$ involve the spin-phonon coupling coefficients C and the phonon integrals I. The C coefficients might be modified, owing to (i) the static distortion of the lattice when Cr^{3+} ions are substituted in the MgO lattice and (ii) the overlap and covalency effects of the ligand charges. Recent calculations by Borg and Ray[20] show that due to the extra charge at the Cr^{3+} site, the Cr^{3+}-O^{2-} distance is reduced by 25% compared to the Mg^{2+}-O^{2-} distance. Using this reduced value of the Cr^{3+}-O^{2-} distance, the value of Z_{eff}, which is obtained by comparing the theoretical value of the static crystal field splitting parameter D with its experimental value, becomes -3.60. If we take this value of Z_{eff} and $R = 1.60$ Å, the magnitudes of the C coefficients are slightly reduced from the values given in Table V. Consequently, this effect can not explain the discrepancy between the experimental and theoretical results of $1/T_1$ for which we require an increase in the magnitude of C. These coefficients might be increased if the covalency and overlap effects are taken into account, which will reduce the gap in the magnitude between the theoretical and experimental values of $1/T_1$. But the fact that Z_{eff} for Cr^{3+} in MgO is nearly equal to the free ionic value of -2 when the static distortions of the lattice is considered, indicates that the covalency and overlap effects are not important in the static case. This implies that one has to justify and show how the overlap and covalency effects might be more important in the dynamical case for Cr^{3+} in MgO.

The I integrals, on the other hand, may be modified by the substitutional effects of the paramagnetic ion in MgO crystal. When a paramagnetic ion is substituted in a perfect lattice, the phonon response functions may change because the mass of the impurity is heavier than that of the host ion and the force constants of the interaction between the magnetic ion and the neighboring O^{2-} ions are different from those between the Mg^{2+} ion and O^{2-} ions.[13] That the anharmonic effects in a crystal may be important in the Raman relaxation time of paramagnetic ions has recently been indicated by Van Kranendonk and Walker.[21] Also, the phonon response functions that were used in the present calculations do not take into account the relative motion between the core and the shell electrons on the ligand ions. This assumption may not be exactly valid for the high-frequency phonons, and that may be one of the reasons for the discrepancies between the two sets of results.

APPENDIX: METHOD OF EVALUATING R FUNCTIONS IN A PERFECT LATTICE

We know that the symmetry-adapted displacements of the complex are expressed in terms of the displacements of the ligand ions by the following relation:

$$Q({}^n\Gamma_\beta^j) = \sum_{\alpha,l,k} A({}^n\Gamma_\beta^j : lk\alpha) u_\alpha(l,k) \ , \tag{A1}$$

where $u_\alpha(l,k)$ denotes the αth component of the displacement of the kth ion in the unit cell labeled by l. Following Born and Huang,[22] these displacement vectors can be transformed to the lattice waves as follows:

$$\begin{aligned} u_\alpha(l,k) = (2/Nm_k)^{1/2} \sum_{\vec{k}}^{N/2} \sum_{p} W_\alpha(k|\vec{k},p) \\ \times [q_1(\vec{k},p)\cos 2\pi \vec{k}\cdot\vec{x}(l,k) \\ - q_2(\vec{k},p)\sin 2\pi\vec{k}\cdot\vec{x}(l,k)] \ , \end{aligned} \tag{A2}$$

where m_k and $\vec{x}(l,k)$ are the mass and the position of the kth ion, respectively. $W_\alpha(k|\vec{k},p)$ is the αth component of the eigenvector of the dynamical matrix, N is the total number of the unit cells in the macrocell, and q_1 and q_2 are the amplitudes of the two standing waves relatively shifted by a quarter wave and p is the branch index. Putting this expression for $u_\alpha(l,k)$ into Eq. (A1), we get

$$Q({}^n\Gamma_\beta^\rho) = \textstyle\sum_s A({}^n\Gamma_\beta^\rho : s) q(s) \ . \tag{A3}$$

The generalized mode index s is equivalent to the index pair (k,p) in the case of the perfect lattice, and the summation over s includes the $N/2$ $\vec{k}$ points. For even-parity modes we have

$$\begin{aligned} A({}^n\Gamma_\beta^\rho : s) = -\sum_{\alpha lk} (2/Nm_k)^{1/2} W_\alpha(k|s) A({}^n\Gamma_\beta^\rho : lk\alpha) \\ \times \sin 2\pi\vec{k}\cdot\vec{x}(l,k) \ , \end{aligned} \tag{A4}$$

$$q(s) = -i(\hbar/4\omega_s)^{1/2}(b_s + b_{-s}^\dagger - b_{-s} - b_s^\dagger) \ ,$$

and for the modes of odd parity

$$\begin{aligned} A({}^n\Gamma_\beta^\rho : s) = -\sum_{\alpha lk} (2/Nm_k)^{1/2} W_\alpha(k|s) A({}^n\Gamma_\beta^\rho : lk\alpha) \ . \\ \times \cos\tfrac{1}{2}\pi\vec{k}\cdot\vec{x}(l,k) \ , \end{aligned} \tag{A5}$$

$$q(s) = \left(\frac{\hbar}{4\omega_s}\right)(b_s + b_{-s} + b_{-s}^\dagger + b_s^\dagger) \ ,$$

where $b_s^\dagger$ and b_s are the creation and the annihilation operators for a phonon of mode s and energy ω_s.

Using Eqs. (13) and the relations (10), we may now calculate the required functions $R_{\Gamma_\beta}^{nn'}(S)$ and, hence, from Eq. (15) the functions $R_{\Gamma_\beta}^{nn'}(\omega)$. It is to be noted that the R functions have no cross products of A (even) and A (odd). Summations over

normal modes are now summations over the Brillouin zone, and the division of the summation as in Eq. (8) implies that we need only consider $\vec{k}$ vectors in the reduced Brillouin zone. The eigenvector components $W_\alpha(k|\vec{k}, p)$ and the eigenvalues $[\omega(\vec{k}, p)]^2$ are found for such $\vec{k}$ vectors using the matrices given by the MgO shell model of Peckham.[9] The number of $\vec{k}$ vectors which are to be included must be sufficient to make sampling errors unimportant.[13]

[1]Jules De Launay, *Solid State Physics* (Academic, New York, 1956), Vol. 2.

[2]J. H. Van Vleck, Phys. Rev. 57, 426 (1940).

[3]J. M. Williams, thesis, University of Bristol, 1962 (unpublished).

[4]C. Y. Huang, Phys. Rev. 139, 241 (1965).

[5]G. H. Larson and C. D. Jeffries, Phys. Rev. 141, 461 (1966).

[6]E. B. Tucker, Phys. Rev. 143, 264 (1966); M. Blume and R. Orbach, *ibid.* 127, 1587 (1966); T. J. Mennes, D. P. Ames, and S. Lee, *ibid.* 169, 333 (1968); I. V. Ovchinnikov, Fiz. Tverd. Tela 5, 1887 (1963) [Soviet Phys. Solid State 5, 1378 (1964)].

[7]R. L. Hartmann, Alfred C. Daniel, J. S. Bennett, and J. G. Castle, Jr., Bull. Am. Phys. Soc. 11, 313 (1966).

[8]J. S. Bennett, R. L. Hartmann, and J. G. Castle, Jr., Bull. Am. Phys. Soc. 11, 483 (1966).

[9]G. Peckham, Proc. Phys. Soc. (London) 90, 657 (1967).

[10]Stephen R. P. Smith, F. Dravnieks, and John E. Wertz, Phys. Rev. 178, 471 (1969).

[11]Santosh Kumar, T. Ray, and D. K. Ray, Phys. Rev. 176, 489 (1968).

[12]I. M. Lifshitz, Nuovo Cimento 3, 716 (1956).

[13]This treatment of Green's functions follows closely that in C. W. McCombie and M. J. L. Sagster (unpublished). Fuller details are given in M. J. L. Sangster, thesis, University of Reading, 1968 (unpublished).

[14]Santosh Kumar, T. Ray, and D. K. Ray, Phys. Status Solidi 37, K65, 1970.

[15]G. F. Koster, J. O. Dimmock, R. G. Wheeler, and Hermann Statz, *Properties of the Thirty-two Point Groups* (M.I.T. Press, Cambridge, Mass., 1963).

[16]W. Low, Phys. Rev. 109, 247 (1958).

[17]E. B. Tucker, Phys. Rev. 143, 264 (1966).

[18]W. Low, Phys. Rev. 105, 801 (1957).

[19]A. J. Freeman and R. E. Watson, Phys. Rev. 120, 1254 (1960); 127, 2058 (1962); S. S. Bishton, M. M. Ellis, D. J. Newman, and J. Smith, J. Chem. Phys. 47, 4133 (1967).

[20]M. Borg and D. K. Ray, Phys. Rev. B 1, 4144 (1970).

[21]J. Van Kranendonk and M. B. Walker, Can. J. Phys. 46, 2441 (1968).

[22]M. Born and K. Huang, *Dynamical Theory of Crystal Lattices* (Oxford U. P., London, 1954).

PHYSICAL REVIEW B VOLUME 2, NUMBER 1 1 JULY 1970

EPR Spectrum of a Jahn-Teller System, NaCl:Cu^{+2}

R. H. Borcherts*

Scientific Research Staff, Ford Motor Company, Dearborn, Michigan 48121

and

H. Kanzaki and H. Abe

Institute for Solid State Physics, University of Tokyo, Minato-ku, Tokyo, Japan

(Received 9 February 1970)

The EPR spectrum of isolated Cu^{+2} ions in NaCl obeys an axial spin Hamiltonian at low temperatures with $g_\parallel = 2.373$, $g_\perp = 2.07$, $A_\parallel = 95$ G, $A_\perp = 40$ G, $Q' = 20$ G with the z axis lying parallel to one of the cube edges. Upon warming toward room temperature, the ligand hyperfine spectrum disappears as the linewidth increases from 16 G at 4.2 K to 25 G at 77 K. At 95-100 K, as this spectrum disappears, a single isotropic line appears with $g = 2.16$ and a linewidth of 60 G. These low- and high-temperature spectra are interpreted as the static and dynamic Jahn-Teller distortions of the CuCl complex. A static strain experiment performed at 77 K results in a repopulation of the three distortion sites and enables a measurement of the strain coefficient V_2 to be made.

INTRODUCTION

As is well known, the ground state of the Cu^{+2} ion ($3d^9$) in an octahedral field splits into a low-lying orbital doublet (E_g) and an excited triplet (T_{2g}) separated by $10Dq$. Because of the ground-state orbital degeneracy, a Jahn-Teller (JT) distortion may occur that will remove the degeneracy and lower the energy of the complex (i.e., the ion and its surrounding ligands).[1] If frozen in this con-